Journal of Environmental Chemical Engineering 5 (2017) 4917–4922

Contents lists available at ScienceDirect

Journal of Environmental Chemical Engineering

journal homepage: www.elsevier.com/locate/jece

Research paper

Arsenate interaction with the surface of nanomagnetic particles. High adsorption or full release

Eliana M. Pecini, Valeria Springer, Maximiliano Brigante, Marcelo Avena*

INQUISUR, Departamento de Química, Universidad Nacional del Sur (UNS)-CONICET, Av. Alem 1253, 8000 Bahía Blanca, Argentina

ARTICLE INFO

Keywords:
Magnetite
Nickel ferrite
Nanoparticles removal
Arsenic
Remediation
Preconcentration

ABSTRACT

The interaction of arsenate species in aqueous media with the surface of nanomagnetic particles with equivalent structure, magnetite (Fe_3O_4) and nickel ferrite ($NiFe_2O_4$), was investigated with adsorption isotherms at pH 4, 7, 9 and 12, desorption kinetics, electrophoresis, XRD, TEM, FTIR, N_2 adsorption and magnetism. Arsenic uptake in both solids was high at pH 4 and decreased as pH increased, becoming negligible at pH 12. The adsorption behavior was typical of anions that form inner-sphere surface complexes with surface metal ions. The reached understanding of the adsorption behavior enabled to achieve, depending on what it is necessary, high and fast adsorption, or complete and rapid desorption by a simple pH change. A flow system was developed for the first time to quantify the ability of a magnetic field to remove nanoparticles with adsorbed arsenate from a dispersion and to measure removal half-lives of the nanoparticles. Both, Fe_3O_4 and $NiFe_2O_4$ exhibited fast and strong responses to the action of the external magnetic field, thus they could be removed in a few minutes with a magnet, leaving a clear and arsenic free solution. The removal half-lives of nanoparticles varied between 75 and 135 s, and were randomly affected by the presence of adsorbed arsenic. These sorptive and magnetic properties make the synthesized nanoparticles useful to be applied in water cleaning technologies and analytical systems, where high adsorption efficiency, fast and complete desorption of arsenic, and full recovery of the adsorbent are needed.

1. Introduction

Highlighting the enormous environmental concern caused by the presence of arsenic (As) in drinking water may sound redundant. However, as long as materials and methodologies that enable efficient removal and accurate quantification of arsenic species are not designed, arsenic in drinking water will keep being a hot topic in chemistry, engineer, medicine and environmental sciences. This is the most common cause of chronic arsenic poisoning in people [1], and it is a serious problem in locations where people depend on groundwater for drinking.

Inorganic arsenic is naturally present at high levels in groundwater in various countries including, Argentina, Bangladesh, Chile, China, Hungary, India, Japan, Mexico, New Zealand, Poland, United States and Vietnam, among others [2]. The World Health Organization (WHO) stablishes a guide value of 10 $\mu g\,L^{-1}$ for drinking water. Therefore, there is a need for the development of highly efficient and easy-to-handle materials and methods to remove arsenic or to quantify it at such low concentrations. A very recent review summarizes structure, characterization methods, mechanisms of action, desorption data, and recent progresses on the applications of magnetic materials for arsenic removal [3]. These materials have generated considerable impact on adsorption and analytical technologies because of their stability, high area/volume ratio and the particular advantage of being separated from aqueous solution in virtue of its magnetism. Magnetic nanoparticles could adsorb arsenic species and leave the aqueous media with concentrations that comply with the WHO guide value. Alternatively, if the nanomaterial reversibly captures and releases arsenic species, it could be used for preconcentration in analytical systems. The possibility of full recovery of the particles by the application of a magnetic field strengthen these and other applications [3].

Nanoscale ferrites (represented by the general formula MFe_2O_4, where M is usually a divalent metal ion) are generally good adsorbents and have interesting magnetic properties [4,5]. Examples of materials with equivalent ferrite structure are nickel ferrite ($NiFe_2O_4$) and magnetite (Fe_3O_4, actually $Fe^{II}Fe^{III}_2O_4$). In addition, they can be easily prepared by the co-precipitation method, making them good candidates for developing adsorbing systems to be used for decontamination or quantification.

The aim of this article is to present a comparative study of arsenate

* Corresponding author.
E-mail address: mavena@uns.edu.ar (M. Avena).

http://dx.doi.org/10.1016/j.jece.2017.09.020
Received 20 June 2017; Received in revised form 3 September 2017; Accepted 9 September 2017
Available online 13 September 2017

adsorption on nickel ferrite and magnetite, both synthesized by co-precipitation. After a general characterization of the synthesized nanoparticles, their interaction with arsenate species in aqueous media was investigated with electrophoretic mobility, adsorption isotherms at pH 4, 7, 9 and 12, and desorption kinetics at high pH, in order to stablish and understand the conditions for high adsorption and fast release. The ability of a magnetic field to remove the synthesized nanoparticles from a dispersion was also investigated with kinetic measurements, and thus removal half-lives of nanoparticles was quantified in absence and presence of adsorbed arsenic.

2. Materials and methods

$FeCl_2{\cdot}4H_2O$ and $FeCl_3{\cdot}6H_2O$ were obtained from Merck (Germany), $NiCl_2{\cdot}6H_2O$ was purchased from Biopack (Argentina). Arsenate stock solutions were prepared by dissolving $Na_2HAsO_4{\cdot}7H_2O$ (Merck, Germany). Methylene Blue was obtained from Merck (Germany), as chloride salt form, and KCl, KOH, HCl were purchased from Anhedra (Argentina). All chemicals were of analytical grade and were used as received. Bidistilled water was used in all cases.

Magnetite particles were synthesized by the chemical coprecipitation method. Specifically, 100 mL of 0.5 M FeCl3 and 100 mL of 0.275 M $FeCl_2$ aqueous solutions were filtered using 0.2 μm pore-diameter cellulose acetate filters (Osmonic), and then mixed and bubbled during 30 min with N_2 in order to remove dissolved CO_2. To obtain the magnetic particles, 107 mL of a 2.05 M NaOH solution were added under vigorous stirring to the mixed iron salts solution in two portions, the first half was added drop by drop (0.5 mL min^{-1}) and the second half quicker (2.0 mL min^{-1}). The pH of the solution was constantly monitored until it was 11. The formed suspension was stirred for a few minutes, and then transferred into 1L of water. The resulting Fe_3O_4 black-brown suspension was washed with water several times to eliminate alkaline impurities from the synthesis, enhancing decantation with a Nd magnet. The suspension was then acidified with HCl to pH 4 to achieve peptization. The resulting stock suspension, whose concentration was determined to be 7.52 g L^{-1}, was stored in the dark at room temperature (~25 °C). The same procedure was followed to synthesize nickel ferrite ($NiFe_2O_4$) particles except that 0.275 M $NiCl_2$ was used instead of $FeCl_2$.

The crystallinity and structure of Fe_3O_4 and $NiFe_2O_4$ were examined by XRD on a Rigaku D-Max III − C instrument equipped with a Cu $K\alpha_1$ (λ = 1.54059 Å) source and a graphite monochromator operated at 35 kV and 15 mA over the 2θ range 3–80° at a scan rate of 0.02° (2θ) s^{-1}. FT-IR spectra were recorded with a Nicolet FT-IR Nexus 470 spectrophotometer in the range from 400 to 4000 cm^{-1} using KBr pellets. The magnetic properties of the samples with and without adsorbed arsenate were measured with a vibrating sample magnetometer (VSM) LakeShore 7404 at room temperature under an applied field of 19000 Oe. The N_2 adsorption isotherms at 77.6 K were measured with a surface area and pore size analyzer (Quantachrome Nova 1200e instrument), wherein the samples were degassed under vacuum during 1 h at 30 °C. TEM was performed with a JEOL 100 CX II microscope, operated at 100 kV with magnification up to 450000×. Observations were made in a bright field.

A Malvern Nano ZS90 equipment was used to measure the electrophoretic mobility of Fe_3O_4 and $NiFe_2O_4$ particles at 25.0 °C. Zeta potential (ζ) data were automatically calculated by the equipment using the Smoluchowski equation. Studies were performed as a function of pH using 10^{-2} M KCl as supporting electrolyte, and the isoelectric point (IEP, pH where ζ = 0) was determined. First of all, 200 mL of a 0.1 g L^{-1} Fe_3O_4 or $NiFe_2O_4$ suspension in 10^{-2} M KCl were prepared. Afterwards, a 50 mL aliquot of this suspension was equilibrated at pH around 3.5 by adding HCl under sonication, continuous stirring and N_2 bubbling in a cylindrical reaction vessel. Once the suspension was stabilized for 30 min, ζ was measured. The pH was then increased with small additions of KOH and ζ was again measured. This procedure was repeated until the pH was around 9.

A similar procedure was employed to evaluate the effect of arsenate on ζ of the studied solids. 50 mL 0.1 g L^{-1} Fe_3O_4 or $NiFe_2O_4$ suspension in 10^{-2} M KCl were equilibrated at pH 9 under continuous stirring and N_2 bubbling. A desired amount of arsenate was then added and ζ at different pH (from 9 to 3) was measured.

Arsenate adsorption isotherms were carried out in 10^{-2} M KCl at pH 4, 7, 9 and 12 using 15 mL polyethylene centrifuge tubes. 0.7 mL of $NiFe_2O_4$ (or 1.0 mL of Fe_3O_4) stock suspension and the desired volume (from 0.1 to 2 mL) of a 1.00×10^{-3} M arsenate solution were mixed in the tubes, and electrolyte solution was added up to a final volume of 10 mL. After 24 h with intermittent sonication and shaking, the suspensions were centrifuged, the supernatant carefully removed and arsenate concentration remaining in the supernatant was quantified by the spectrophotometric molybdene blue method validated by Lenoble et al. [6] for arsenic species in aqueous media. We have made an evaluation of the performance of the method under our experimental conditions, and the results are shown as Supplementary material. The limit of detection, 3.97×10^{-7} M (30 ppb As), was adequate for the requirements of the present work. Adsorbed arsenate was calculated as the difference between the initial arsenate concentration and the equilibrium arsenate concentration that remained in the supernatant.

In order to evaluate the possibility of reusing the magnetic particles, arsenate desorption experiment were conducted at pH 9 and 12. First, arsenate adsorption was carried out at pH 4, as indicated above, but using 60 mL of a 0.75 g L^{-1} Fe_3O_4 suspension (0.83 g L^{-1} $NiFe_2O_4$ suspension) in 10^{-2} M KCl. Once adsorption equilibrium was achieved, the pH was quickly increased to 9 or 12 by adding KOH, and then 5 mL aliquots were withdrawn at different times to monitor the desorption kinetics. The pH was continuously checked and kept constant at the corresponding desorption value.

Finally, a method was developed to analyze the ability of the synthesized magnetic nanoparticles to be removed from suspension by a magnet. 50 mL of a 0.1 gL^{-1} Fe_3O_4 or $NiFe_2O_4$ suspension in 10^{-2} KCl at pH 7 were maintained in a cylindrical glass vessel under stirring and N_2 bubbling. A Gilson Minipuls 8 peristaltic pump was used to flow the suspension from the vessel to the spectrophotometer cell, where the turbidity (τ) or the absorbance (A) was continuously monitored. A close flow system was used in these experiments, meaning that the suspension flowed through the cell and back to the vessel after τ or A reading. The experiment was started by flowing the suspension in absence of a magnet, with turbidity remaining constant and maximum. A Nd magnet was then attached to the external face of the vessel wall so that the particles became retained by the magnetic field. This caused a continuous decrease in the turbidity, which allowed to plot turbidity vs. time curves and to estimate the rate of particles removal by the field. The turbidity or absorbance was monitored at 480 nm.

3. Results and discussion

Fig. 1 shows the X-ray diffractograms of Fe_3O_4 and $NiFe_2O_4$. The pattern of the Fe_3O_4 sample dried at 25 °C matched that of pure magnetite (ICDD: 00-019-0629), exhibiting the characteristics peaks at 30.2° (220), 35.2° (311), 43.2° (400), 53.7° (422), 57.1° (511), 62.7° (440), 70.9° (620), and 74.4° (533). $NiFe_2O_4$ showed to be a poorly crystallized material even after drying at 105 °C, with a pattern similar to that of akaganeite, $(Fe^{3+}, Ni^{2+})_8(OH,O)_{16}Cl_{1.25}{\cdot}nH_2O$ (ICDD: 00-042-1315). Only after calcination at 600 °C the characteristic diffractogram of nickel ferrite (ICDD: 00-054-0964) was recorded and no other crystalline phases were detected. This pattern showed diffraction peaks at 30.3° (220), 35.6° (311), 37.3° (222), 43.3° (400), 53.8° (422), 57.3° (511), 63.0° (440), 71.5° (620), 74.5° (533) and 75.4° (622). Since only calcination at 600 °C produced the solid with the desired $NiFe_2O_4$ structure, this calcined sample was employed in further studies and compared to Fe_3O_4.

In order to determine the crystallite size (*D*), a line profile analysis

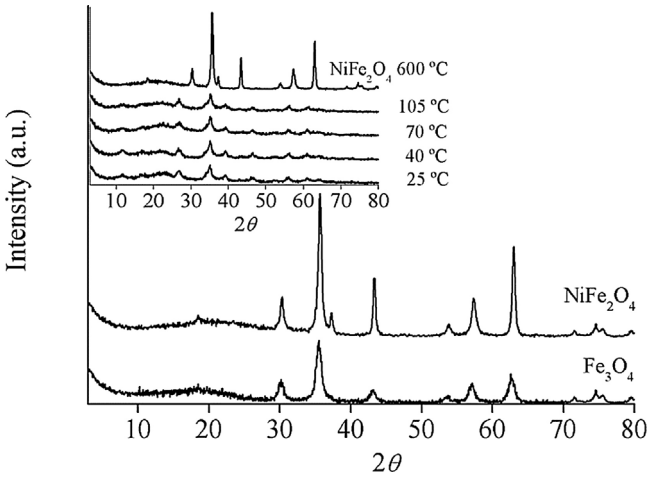

Fig. 1. XRD patterns of synthesized Fe_3O_4 (dried at 25 °C) and $NiFe_2O_4$ (calcined at 600 °C). Changes in the XRD patterns of $NiFe_2O_4$ after drying in the 25–105 °C temperature range and after calcining at 600 °C are shown in the inset of the figure.

was performed on the diffractograms using the Scherrer equation:

$$D = \frac{K\lambda}{\beta\cos(\theta)}$$

Where K is the so-called shape factor (Scherrer constant), λ is the wavelength of the X-ray source, β the line width at half maximum intensity in radians and θ is the Braggś angle in degrees units. Using the linewidth of the (311) reflection, D_{311} was calculated to be 12.0 nm for $Fe_3O_4$and 16.6 nm for $NiFe_2O_4$. These sizes are comparable with data reported in the literature for Fe_3O_4 [7] and $NiFe_2O_4$ particles [8] and agree also with TEM micrographs (Fig. 2), which show that magnetite nanoparticles are somewhat smaller than nickel ferrite nanoparticles.

Fig. 3 shows the FTIR spectra of the studied solids. Fe_3O_4 particles exhibit two absorption bands at 581 and 440 cm^{-1} due to Fe—O stretching vibrations in tetrahedral and octahedral positions, respectively. Similarly, the IR spectrum of $NiFe_2O_4$ shows two broad metal–oxygen (M—O) stretching bands: one at 604 cm^{-1}, corresponding to the metal in tetrahedral location, and the other one at 425 cm^{-1}, assigned to the metal in octahedral position [9,10]. The spectrum of Fe_3O_4 also shows a broad and intense absorption band at 3400 cm^{-1} due to O—H stretching vibrations, and a band at 1644 cm^{-1} due to the O—H bending vibration, both indicating the presence of some remnant water as the results of drying only at 25 °C.

The nitrogen adsorption-desorption isotherms and BJH pore-size distributions of the solids are presented in Fig. 4. The BET surface areas were 108 and 37 $m^2 g^{-1}$ for Fe_3O_4 and $NiFe_2O_4$, respectively. The average pore volume and the average pore radius were 0.17 $cm^3 g^{-1}$ and 3.41 nm for Fe_3O_4, and 0.33 $cm^3 g^{-1}$ and 15 nm for $NiFe_2O_4$. In both cases, the solids show II-type isotherms according to IUPAC classification, characteristic of nonporous or macroporous materials. At

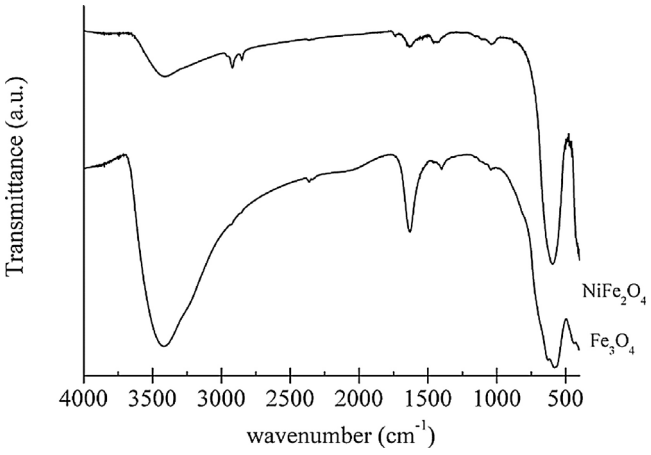

Fig. 3. FTIR spectra of the studied Fe_3O_4 and $NiFe_2O_4$ nanoparticles.

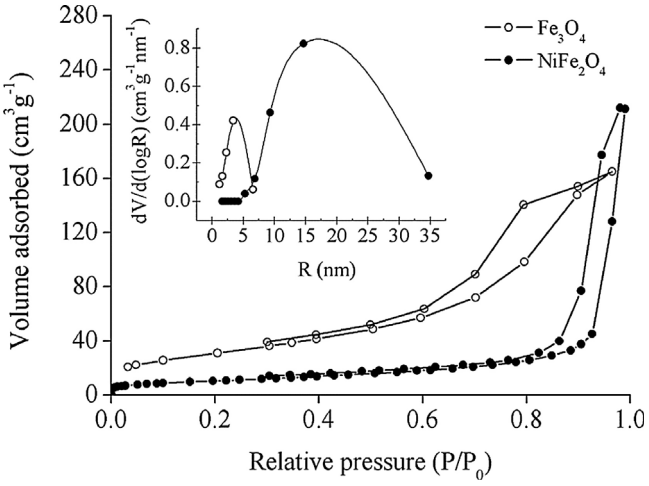

Fig. 4. Nitrogen adsorption-desorption isotherms of studied nanoparticles. The inset shows their pore size distribution.

higher relative pressure ($P/P0 > 0.9$), a narrow hysteresis due to the porosity between particles can be observed [11].

The room temperature magnetization curves of Fe_3O_4 and $NiFe_2O_4$ particles with and without adsorbed arsenate are shown in Fig. 5. The saturation magnetization (M_s) for pure Fe_3O_4 was 67.8 emu g^{-1}. This value is lower than for bulk multidomain Fe_3O_4 (85–100 emu g^{-1}) [12] but is comparable with those reported for nanosized particles [13,14]. Magnetite nanoparticles showed a typical superparamagnetic behavior, as evidenced by a negligible value of both the remanence magnetization (M_r = 0.16 emu g^{-1}) and the coercivity field (H_c = 1.0 Oe) [15]. This means that room temperature is sufficient to disrupt the magnetic spins instantly after the external field is removed. The magnetic properties

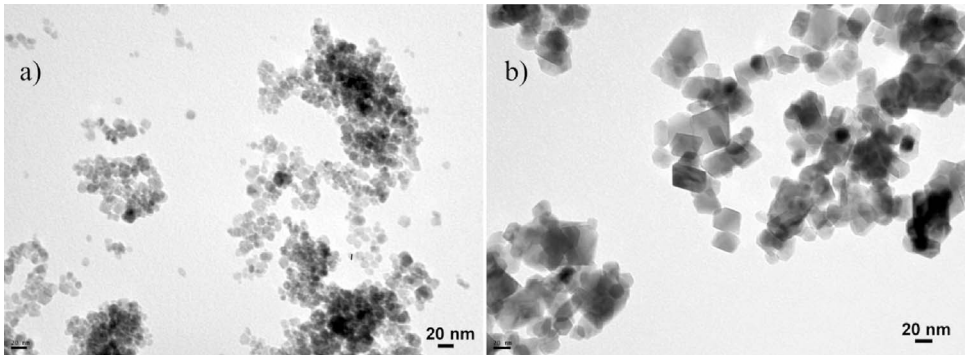

Fig. 2. TEM micrographs of the studied samples. (a) Fe_3O_4, (b) $NiFe_2O_4$.

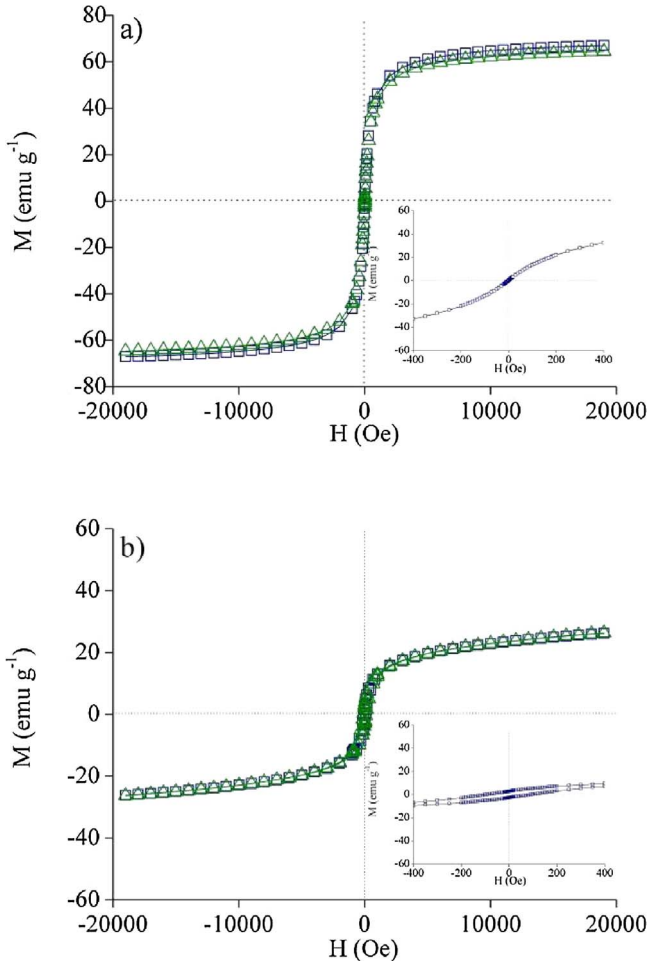

Fig. 5. Magnetization curves of the studied samples as a function of magnetic field applied at room temperature. Different symbols correspond to solids with adsorbed As(V) at different percentages of surface saturation: squares, 0%; triangles, 60%. pH = 7. The inset of the figure shows the expanded regions around the origin for samples without adsorbed As(V).

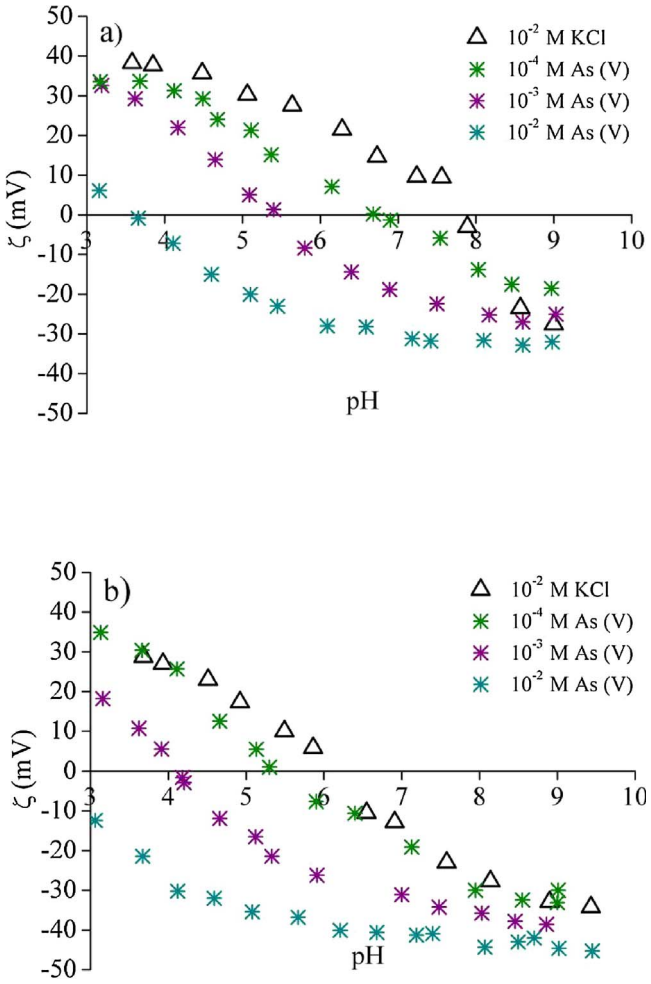

Fig. 6. a) ζ vs pH for Fe_3O_4. Triangles, in 10^{-2} M KCl; stars, in 10^{-2} M KCl with different arsenate concentrations (given in the figure). b) Idem for $NiFe_2O_4$ particles.

did not change when arsenic species were adsorbed.

Magnetization curve of pure $NiFe_2O_4$ shows that the sample has a typical ferromagnetic behavior [9]. In this case saturation magnetization was not reached, and the reported value of M_s (25 emu g^{-1}) corresponds to the maximum applied field. Anew, this value is significantly lower than that of the multidomain bulk particles (55 emu g^{-1}) [16], but is comparable with that reported for nanosized particles [17], since it is well known that for magnetic particles the size has significant influence on their magnetic properties [18,19]. Finally, H_c and M_r of the $NiFe_2O_4$ nanoparticles were respectively 100 Oe and 2.7 emu g^{-1}. The magnetic properties did not change significantly when arsenic species were adsorbed. As a summary, magnetic properties of both Fe_3O_4 and $NiFe_2O_4$ indicate that the synthesized nanoparticles can be easily removed from a reaction vessel using a conventional magnet, and easily redispersed by withdrawing the magnet. This can be done to the particles with or without adsorbed arsenic.

Fig. 6a shows the electrokinetic behavior of Fe_3O_4 at different pH. In absence of arsenate, curves at three different ionic strengths resulted in an isoelectric point (IEP) of 7.8, in agreement with the literature [20]. In the presence of arsenate and at constant ionic strength (10^{-2} M KCl) the IEP shifted to 7.0, 5.5, and 3.5 for arsenate concentrations 10^{-4}, 10^{-3}, 10^{-2} M, respectively. Fig. 6b shows a similar behavior for $NiFe_2O_4$, which had an IEP of 6 in absence of arsenate, in agreement with the literature [21], and IEPs that shifted to 5.4, 4.0 and < 3.0 for arsenate concentrations 10^{-4}, 10^{-3}, 10^{-2} M, respectively. The behavior of both materials is typical of solids with surfaces that specifically adsorb anions, arsenate species in this case, forming inner-sphere surface complexes [22].

Arsenate adsorption isotherms at pH 4, 7, 9 and 12 in 10^{-2} M KCl are shown in Fig. 7. The adsorption decreased as pH increased, becoming negligible at pH 12. In agreement with electrokinetic results, the behavior is typical of specifically adsorbing anions on variable charge surfaces. It is well known that arsenate adsorbs strongly on metal oxides forming inner-sphere surface complexes with metal ions at the solid surface. These complexes are the result of a ligand exchange reaction, where surface hydroxyls and/or water molecules are replaced by arsenate species. The adsorption is usually well described by surface complexation models such as Triple Layer Model [23] or CD-MUSIC model [24,25], which consider ligand exchange and electrostatic interactions between surface and adsorbing ions. The combined effect of ligand exchange and electrostatics leads to the observed decrease in adsorption as pH increased and the decrease in IEP as arsenate concentration increased [26]. In a per gram basis, magnetite nanoparticles adsorbed more As(V) than nickel ferrite. At pH 4.0, for example, the uptake was 194 μmol g^{-1} on Fe_3O_4 and 130 μmol g^{-1} on $NiFe_2O_4$. In a per square meter basis, on the contrary, nickel ferrite adsorbed more (1.80 μmol m^{-2} on Fe_3O_4 and 3.51 μmol m^{-2} on $NiFe_2O_4$, pH = 4.0), as a consequence of the almost 3-times lower surface area of nickel ferrite. We have no explanation thus far on the reason why a given area of the ferrite seems to be more active than a same area of magnetite. A pure electrostatic analysis would indicate that Fe_3O_4 should capture better arsenate species per unit surface than $NiFe_2O_4$ because the IEP of

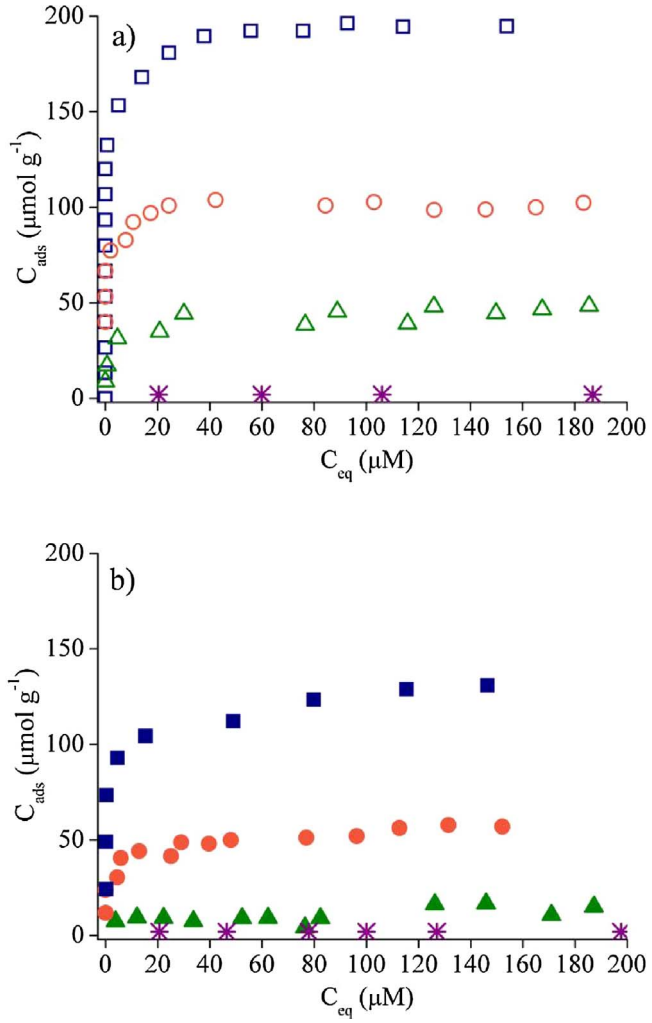

Fig. 7. a) As(V) adsorption isotherms on Fe_3O_4 at different pH: squares, pH 4; circles, pH 7; triangles, pH 9; stars, pH 12. C_{ads} represents adsorbed amount of As(V), and C_{eq} is its corresponding equilibrium concentration in the supernatant. b) Idem for $NiFe_2O_4$ nanoparticles.

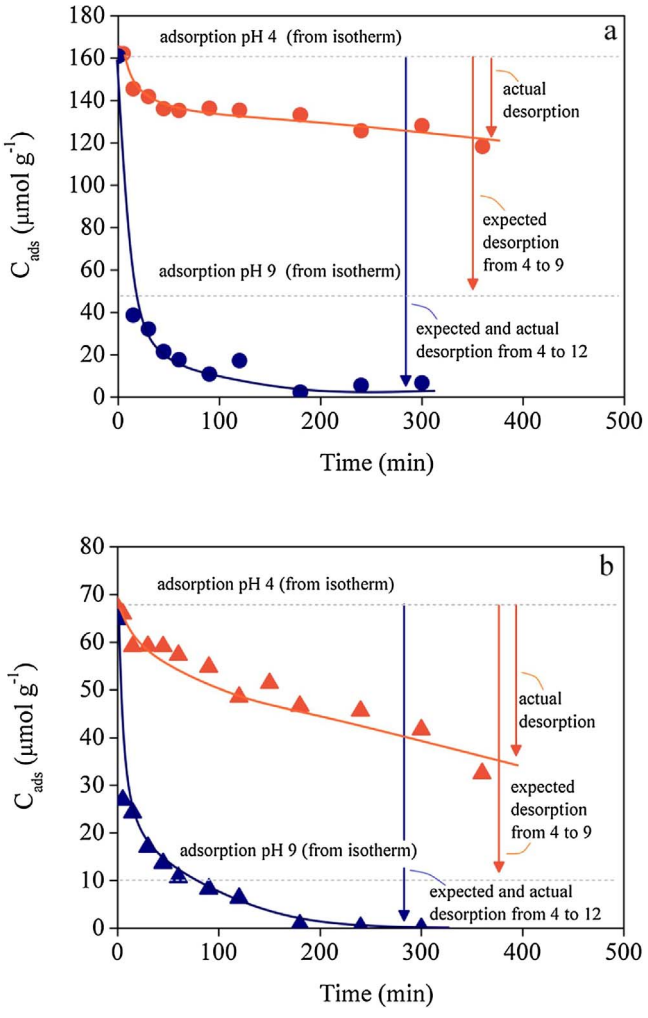

Fig. 8. a) Desorption of As(V) from Fe_3O_4. Initial adsorption pH: 4; initial arsenate concentration: 1.6×10^{-4} M; orange symbols: desorption at pH 9; blue symbols: desorption at pH 12. Equilibrium adsorption values from isotherms at pH 9 and 12 are shown with dotted lines, and actual and expected desorption from pH 4 to 9 are indicated with orange arrows. Actual and expected desorption from pH 4 to 12 nearly coincide and are indicated with only one blue arrow. Temperature: 25 °C; stirring rate: 520 rpm. b) idem for $NiFe_2O_4$, except that the initial arsenate concentration was 8.0×10^{-5} M. (For interpretation of the references to colour in this figure legend, the reader is referred to the web version of this article.)

the former is higher than that of the later. Differences in surface site densities cannot explain the behavior either, since structures are equivalent and site densities should be very similar. The behavior appears to be of physical origin, due to differences in areas accessible to nitrogen (the probe molecule in BET analysis) and arsenate species. The much smaller pores of Fe_3O_4 may be freely accessible to nitrogen in a gas-solid experiment but not so easily accessible to arsenate and water molecules in the arsenate adsorption experiments, whereas the larger pores of the ferrite should be equally accessible to both, nitrogen and arsenate.

Fig. 8 shows the results obtained from desorption studies by increasing the pH to 9 or 12 after adsorbing at pH 4. There was desorption at both pH for both solids. In the case of desorbing at pH 9, it should be remarked that desorption must not be complete under the investigated conditions. In a batch system, every desorbed arsenate ion contributes to increase arsenate concentration in solution, and thus the desorption reaction must stop when the new equilibrium situation at pH 9 is reached. This new equilibrium situation is dictated by the adsorption isotherms at pH 9, and marked by a dotted line in the figure. The expected and actual extents of desorption by rising the pH from 4 to 9 and from 4 to 12 are given by arrows. Data indicates that desorption at pH 9 for both Fe_3O_4 and $NiFe_2O_4$ did not reach the new equilibrium situations even after 6 h, showing a poor desorption efficiency. In the case of desorbing at pH 12, near complete desorption was expected for both solids since adsorption isotherms at that pH revealed a negligible adsorption. Within experimental errors, Fig. 8 shows that desorption at pH 12 was rather fast and efficient, achieving indeed near complete desorption after 3 h.

Adsorption systems containing magnetic particles as the adsorbing entities are technologically interesting because the particles and thus the adsorbed substances can be easily removed from the dispersion using an external magnet. This is currently demonstrated in the literature with pictures showing that before applying the magnet all particles were dispersed, and that after applying it the particles became attracted by the magnetic field, leaving a clear solution, which is the desired final situation. However, information about the time needed to achieve this final situation is not always reported. The method developed in this paper enables to investigate the kinetics of nanoparticles removal, by plotting the normalized absorbance (A/A_0), or the normalized turbidity (τ/τ_0), as a function of time after applying the magnetic field. The obtained results are shown in Fig. 9. In all cases, nanoparticles (with or without adsorbed arsenate) could be readily removed with the magnet. Since the suspension in the vessel was kept under stirring, there was no possibility for sedimentation and thus all

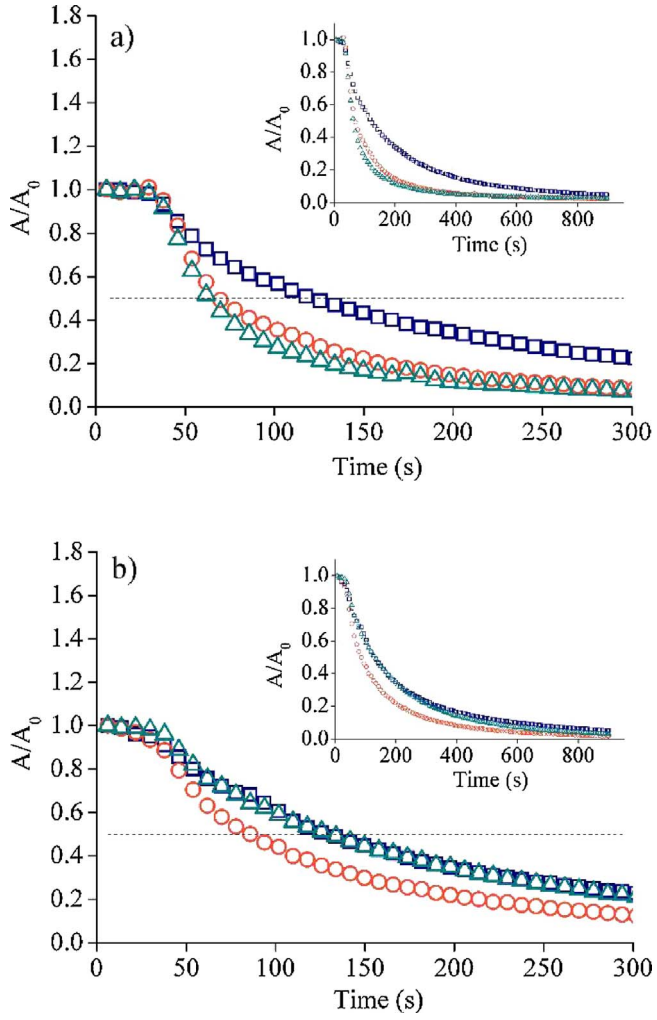

Fig. 9. Normalized optical absorbance (A/A_0) of nanoparticles suspensions as a function of time with different amount of adsorbed As(V) under the influence of an external magnetic field. a) Fe_3O_4, b) $NiFe_2O_4$. All suspensions were prepared in 10^{-2} KCl, pH = 7. Different symbols correspond to solids with adsorbed As(V) at different percentages of surface saturation: squares, 0%; circles, 20%; triangles, 60%.

decrease in absorbance corresponded to removal by the magnet. There was no special trend in the removal half-lives (time needed to decrease absorbance by 50%). Half-lives between 75 s and 135 s were observed. In most cases 800 s were enough to completely remove the nanoparticles obtaining a clear solution.

The results of this work show that synthesized Fe_3O_4 and $NiFe_2O_4$ nanoparticles are very good As(V) adsorbents in aqueous media, they can desorb all As(V) if desired, and can also be attracted and removed from suspensions with a normal magnet. These properties make them suitable to be used and reused in, for example, decontaminating technologies [27,28] or analytical systems [29,30]. In the first case, As(V) species contaminating drinking water can be adsorbed on the nanoparticles, and both, nanoparticles and arsenic removed from water. Keeping the pH between 4 and 7 in these systems will be enough to achieve an efficient adsorption. A simple washing at high pH will remove all adsorbed arsenic from the solid, leaving the nanoparticles ready for reuse. In the second case, they could be applied in analytical methods where preconcentration of As(V) is necessary before quantification. In this sense, a flow system can be constructed, with arsenical water flowing through the nanoparticles, which are retained by a magnetic field. Nanoparticles will preconcentrate the analyte between low and circumneutral neutral pH, and release it to the detector by a simple desorption at high pH. If it is necessary, after several quantification cycles nanoparticles could be easily replaced by new ones by switching on-off the magnetic field.

4. Conclusions

The present study shows that Fe_3O_4 and $NiFe_2O_4$ nanoparticles can be easily synthesized and used as As(V) adsorbent in aqueous media. Besides a thorough characterization of the solids, adsorption isotherms at different pH showed that arsenic uptake is important at pH 4 and decreases as pH increases, becoming negligible at pH 12. These equilibrium data give the theoretical basis for achieving an effective desorption process at pH 12, where all adsorbed arsenic is efficiently released to the solution.

A flow system was developed for the first time to quantify the ability of a magnetic field to remove nanoparticles from a dispersion. Both, Fe_3O_4 and $NiFe_2O_4$ nanoparticles exhibit fast and strong responses to the action of the external magnetic field, thus they could be removed in a few minutes with a magnet, leaving a clear and arsenic free solution.

Due to their magnetic properties, and to their high As(V) adsorption capacity at low pH and fast and complete desorption at high pH, the synthesized nanoparticles are suitable to be used in decontaminating or analytical systems, where high adsorption efficiency, complete desorption of analytes, and full recovery of the adsorbent are needed.

Acknowledgments

This work was financed by CONICET, FONCyT and UNS. E.P and V.S thank CONICET for the doctoral and postdoctoral fellowships.

Appendix A. Supplementary data

Supplementary data associated with this article can be found, in the online version, at http://dx.doi.org/10.1016/j.jece.2017.09.020.

References

[1] P.L. Smedley, D.G. Kinniburgh, Appl. Geochem. 17 (2002) 517–568.
[2] B.K. Mandal, K.T. Suzuki, Talanta 58 (2002) 201–235.
[3] A. Jabasingh, T. Ravi, A. Yimman, Water Sci. (2017) (in press).
[4] M. Ashtar, A. Munir, M. Anis-Ur-Rehman, A. Maqsood, Mater. Res. Bull. 79 (2016) 14–21.
[5] K. Ahalya, N. Suriyanarayanan, V. Ranjithkumar, J. Magn. Magn. Mater. 372 (2014) 208–213.
[6] V. Lenoble, V. Deluchat, B. Serpaud, J.-C. Bollinger, Talanta 61 (2016) 267–276.
[7] S. Laurent, D. Forge, M. Port, A. Roch, C. Robic, L.V. Elst, R.N. Muller, Chem. Rev. 108 (2008) 2064–2110.
[8] S.L. Darshane, S.S. Suryavanshi, I.S. Mulla, Ceram. Int. 35 (2009) 1793–1797.
[9] M. Salavati-Niasari, F. Davar, T. Mahmoudi, Polyhedron 28 (2009) 1455–1458.
[10] A. Adam, Z. Ali, E. Abdeltwab, Y. Abbas, Optoelectron. Adv. Mater. 3 (2009) 1195–1199.
[11] I. Ursachi, A. Vasile, H. Chiriac, P. Postolache, A. Stancu, Mater. Res. Bull. 46 (2011) 2468–2473.
[12] C. Han, D. Zhao, C. Deng, K. Hu, Mater. Lett. 70 (2012) 70–72.
[13] K. Petcharoen, A. Sirivat, Mater: Sci. Eng. B Solid-State Mater. Adv. Technol. 177 (2012) 421–427.
[14] Y.S. Kang, S. Risbud, J.F. Rabolt, P. Stroeve, Chem. Mater. 8 (1996) 2209–2211.
[15] H. Li, L. Qin, Y. Feng, L. Hu, C. Zhou, J. Magn. Magn. Mater. 384 (2015) 213–218.
[16] H. Nathani, S. Gubbala, R.D.K. Misra, Mater. Sci. Eng. B 121 (2005) 126–136.
[17] A.P.G. Rodrigues, D.K.S. Gomes, J.H. Araújo, D.M.A. Melo, N.A.S. Oliveira, R.M. Braga, J. Magn. Magn. Mater. 374 (2015) 748–754.
[18] a Demortière, P. Panissod, B.P. Pichon, G. Pourroy, D. Guillon, B. Donnio, S. Bégin-Colin, Nanoscale 3 (2011) 225–232.
[19] R.K. Panda, R. Muduli, D. Behera, J. Alloys Compd. 634 (2015) 239–245.
[20] E. Illés, E. Tombácz, J. Colloid Interface Sci. 295 (2006) 115–123.
[21] M. Kosmulski, Adv. Colloid. Interface Sci. 171–172 (2012) 77–86.
[22] S. Hokkanen, E. Repo, S. Lou, M. Sillanpää, J. Chem. Eng. 260 (2015) 886–894.
[23] J. Davis, R. James, J. Leckie, J. Colloid Interface Sci. 63 (1978) 480–499.
[24] T. Hiemstra, W.H. Van Riemsdijk, J. Colloid Interface Sci. 210 (1999) 182–193.
[25] J. Antelo, M. Avena, S. Fiol, R. López, F. Arce, J. Colloid Interface Sci. 285 (2005) 476–486.
[26] W. Stumm, Chemistry of the Solid-water Interface, John Wiley and Sons, New York, 1992.
[27] E. Bringas, J. Saiz, I. Ortiz, Sep. Purif. Technol. 156 (2015) 699–707.
[28] H.L. Fan, L. Li, S.F. Zhou, Y.Z. Liu, Ceram. Int. 42 (2016) 4228–4237.
[29] Y. Moliner-Martínez, A. Ribera, E. Coronado, P. Campíns-Falcó, J. Chromatogr. A 1218 (2011) 2276–2283.
[30] A.A. Ensafi, S. Rabiei, B. Rezaei, A.R. Allafchian, Anal Methods 5 (2013) 3903.